Published in final edited form as:

Biochemistry. 2016 June 14; 55(23): 3234–3240. doi:10.1021/acs.biochem.6b00292.

Photochemical Generation of a Tryptophan Radical within the Subunit Interface of Ribonucleotide Reductase

Lisa Olshansky[a,b], **Brandon L. Greene**[a], **Chelsea Finkbeiner**[b], **JoAnne Stubbe**[b], and **Daniel G. Nocera**[a]

[a] Department of Chemistry and Chemical Biology, 12 Oxford Street, Cambridge, MA 02138–2902; dnocera@fas.harvard.edu

[b] Department of Chemistry, Massachusetts Institute of Technology, 77 Massachusetts Avenue, Cambridge, MA 02139-4307; stubbe@mit.edu.

Abstract

The *E. coli* class Ia ribonucleotide reductase (RNR) achieves forward and reverse proton-coupled electron transfer (PCET) over a pathway of redox-active amino acids (β-Y_{122} ⇋ β-Y_{356} ⇋ α-Y_{731} ⇋ α-Y_{730} ⇋ α-C_{439}) spanning ~35 Å and two subunits every time it turns over. We have developed photoRNRs that allow radical transport to be phototriggered at tyrosine (Y) or fluorotyrosine (F_nY) residues along the PCET pathway. We now report a new photoRNR in which photooxidation of a tryptophan (W) residue replacing Y_{356} within the α/β subunit interface proceeds by a stepwise ETPT (electron transfer then proton transfer) mechanism and provides an orthogonal spectroscopic handle with respect to radical pathway residues Y_{731}/Y_{730} in α. This construct displays a ~3-fold enhancement in photochemical yield of W• relative to F_3Y• and a ~7-fold enhancement relative to Y•. Photogeneration of the W• radical occurs with a rate constant of $4.4 \pm 0.2 \times 10^5$ s^{-1}, which obeys a Marcus correlation for radical generation at the RNR subunit interface. Despite the fact that the Y → W variant displays no enzymatic activity in the absence of light, photogeneration of W• within the subunit interface results in 20% activity for turnover relative to wt-RNR under the same conditions.

Abstract

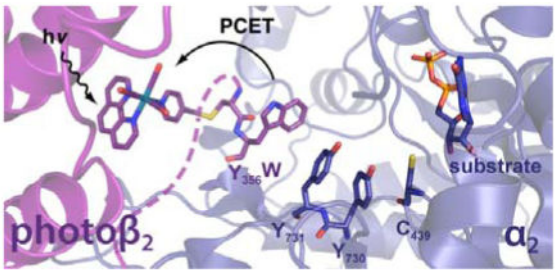

Supporting Information

Supporting information available including a detailed materials and methods description and emission lifetime traces.

Ribonucleotide reductase (RNR) catalyzes the conversion of nucleotides to deoxynucleotides in all organisms, providing the monomeric building blocks for DNA replication and repair. The class Ia RNR from *E. coli* is composed of two homodimeric subunits, α_2 which contains the active site and β_2 which houses the $Fe^{III}_2(\mu\text{–}O)/Y_{122}\bullet$ cofactor required to initiate active site radical chemistry.[1] The active oligomeric state is an $\alpha_2\beta_2$ complex[2–4] that comes together transiently during turnover to accomplish long-range (~35 Å) radical translocation over a pathway of redox active amino acids ($\beta\text{-}Y_{122} \leftrightharpoons \beta\text{-}Y_{356} \leftrightharpoons \alpha\text{-}Y_{731} \leftrightharpoons \alpha\text{-}Y_{730} \leftrightharpoons \alpha\text{-}C_{439}$) via a series of individual proton-coupled electron transfer (PCET) hopping steps.[5,6]

Pre-steady state kinetics of RNR turnover reveal that the rate-determining step in this mechanism is a conformational change triggered by substrate binding that occurs at 2–10 s^{-1}.[7] In order to study the kinetics of individual PCET steps during turnover, we have developed methods to initiate radical transport within RNR photochemically.[8–10] Installation of a bromomethylpyridyl rhenium(I) tricarbonyl phenanthroline complex ($[Re^I]$) at position β_{355} via cysteine ligation produces a photoβ_2,[11] where the adjacent Y_{356} has been replaced with various fluorotyrosines (F_nYs, n = 2–3) to modulate the pK_a and $E^{\circ\prime}$ of Y_{356} within the RNR subunit interface.[12,13] This methodology has enabled spectroscopic observation of photochemically competent radical intermediates,[9,12] assignment of rate constants associated with individual PCET steps,[12] and determination of Marcus parameters within the α/β subunit interface.[13] In these studies, individual Y• species from among the $\beta\text{-}Y_{356}$, $\alpha\text{-}Y_{731}$ and $\alpha\text{-}Y_{730}$ triad could not be spectroscopically resolved, preventing measurement of PCET rates among them. In one approach toward unraveling the PCET kinetics associated with the tyrosine triad, a Y_{356}W-photoβ_2 construct has been prepared. We show that photoinitiation of Y_{356}W-photoβ_2 yields a $\bullet W_{356}$ radical absorption feature that is well-resolved from that of Y•. With this Y_{356}W-photoβ_2, we have begun to disentangle individual PCET kinetics among the $\beta\text{-}Y_{356} \leftrightharpoons \alpha\text{-}Y_{731} \leftrightharpoons \alpha\text{-}Y_{730}$ triad of RNR. We show that the rate for radical generation within the amino acid triad is described well by a Marcus treatment of charge transport.

Materials and Methods

Wt-α_2 (2,000 nmol/mg/min) and $Y_{731}F\text{-}\alpha_2$ were expressed and purified as previously described.[14] All α_2 proteins were pre-reduced prior to use by incubation with 30 mM DTT for 30 min at RT followed by buffer exchange. [5-^{3}H]-cytidine 5′-diphosphate sodium salt hydrate ([5-^{3}H]-CDP) was purchased from ViTrax (Placentia, CA), Tricarbonyl(1,10-phenanthroline)(4-bromomethyl-pyridine)rhenium(I) hexafluorophosphate ($[Re^I]$–Br) was available from a previous study.[11] *E. coli* thioredoxin (TR, 40 μmol/min/mg) and thioredoxinreductase (TRR, 1,800 μmol/min/mg) were prepared as previously described.[15,16] $C_{268}S/C_{305}S/S_{355}C/Y_{356}W\text{-}\beta_2$ and $Y_{356}W\text{-}\beta_2$ were generated by site-directed mutagenesis using the primers described in the SI, and expressed and purified as previously reported for related photoβ_2 variants.[12] All photoβ_2s were reduced with hydroxyurea prior to measurements to eliminate the native tyrosyl radical cofoactor. $C_{268}S/C_{305}S/S_{355}C/Y_{356}F\text{-}\beta_2$ was available from a previous study.[12] Assay buffer consists of 50 mM HEPES, 15 mM $MgSO_4$ and 1 mM EDTA adjusted to pH 7.6.

Photochemical turnover experiments were performed as previously reported under two conditions, those similar to TA spectroscopy (in the presence of 10 mM $Ru(NH_3)_6Cl_3$), and those similar to emission quenching measurements (in the absence of $Ru(NH_3)_6Cl_3$).[12] In each case, 10 μM of either Y_{356}W- or Y_{356}F-photoβ_2 was mixed with either wt- or Y_{731}F-α_2 (10 μM), 0.2 mM [5-^{3}H]-CDP (specific activity 26,700 cpm/nmol), 1 mM ATP, and with or without 10 mM $Ru(NH_3)_6Cl_3$ in assay buffer at pH 7.6. Samples were placed in a 4 mm × 4 mm quartz cuvette and held at 25 °C under illumination for 10 min with white light powered at 800 W (35 V and 24 A DC) in conjunction with a 313 nm long-pass cutoff filter. Quantitation of radioactive products by scintillation counting was performed as previously described.[10,12,17] The data presented are averages of 3 independently prepared samples, and error bars represent one standard deviation (s.d.).

Nanosecond spectroscopy was performed using a modified version of a previously reported home-built Nd:YAG laser system.[9] In the modified setup, the previously used Triax 320 spectrometer has been replaced by a Horiba iHR320 spectrometer. Optical long-pass cutoff filters (λ > 375 nm) were used to filter probe light before detection to remove scattered 355 nm pump light. The reported experiments used a 250 nm blaze grating (300 grooves/mm). The power of the pump beam (λ = 355 nm) was set to 2 mJ/pulse.

For transient absorption (TA) spectra, the output of the Xe-arc lamp was set to 3.0 ms pulses with 30 A current. TA spectra and kinetic traces are the averages of measurements made from 1000 laser shots (500 four spectrum sequences in the case of the TA spectra) on 3 independently prepared samples. TA samples were prepared in a total volume of 650 μL and recirculated through a 1 cm path length flow-cell to reduce sample decomposition. An inline filter (Acrodisc 13 mm 0.2 μM Supor Membrane, Pall Corporation) was used to collect solid photoproducts. Samples contained either 50 μM Y_{356}W-photoβ_2 with and without 75 μM wt-α_2, or 30 μM Y_{356}F-photoβ_2 with and without 50 μM wt-α_2, and 1 mM CDP, 3 mM ATP and 10 mM $Ru(NH_3)_6Cl_3$ in assay buffer at pH 7.6. Single wavelength kinetics data were collected at 520 or 560 nm using slit widths corresponding to ±1 nm resolution and least-squares fitting was performed using the OriginPro 8.0 data analysis software over 3–80 μs according to Eq. 1, accounting for the instrument response and radical decay.

$$y = y_\circ + A_1 e^{-\tau/t_1} + A_2 e^{-\tau/t_2} \quad (1)$$

Emission quenching experiments were prepared in a total volume of 550 μL and recirculated through a 1 cm path length flow-cell to reduce sample decomposition. Samples contained 10 μM Y_{356}W- or Y_{356}F-photoβ_2, 1 mM CDP, 3 mM ATP, with or without 25 μM wt- or Y_{731}F-α_2, in assay buffer at pH 7.6. Single wavelength kinetics data were collected at 600 nm using slit widths corresponding to ±0.75 nm resolution and recorded over 1000 laser shots for each sample. Lifetime data were obtained in triplicate with independently prepared samples for each experimental condition and least-squares fitting were performed using the OriginPro 8.0 data analysis software over the 0.1–4.5 μs time window according to Eq. 2.

$$y = y_{\circ} + A_1 e^{-\tau/t} \quad (2)$$

Triplicate measurements were performed in all cases and error associated with the goodness of fit, as well as that between replicates, was propagated. Calculation of k_q is achieved by applying Eq. 3, where the inverse of the excited state lifetimes measured in the presence of Y_{356}W- and Y_{356}F-photoβ_2s (τ_W and τ_F, respectively) are subtracted. Eq. 4 was used to propagate error, where σ_W and σ_F are the standard deviations for the triplicate measurements of each (compounded with error associated with the goodness of fit), and δ is the final reported error k_q.

$$k_q = \frac{1}{\tau_W} - \frac{1}{\tau_F} \quad (3)$$

$$\delta = \sqrt{\left(\frac{\sigma_W}{\tau_W^2}\right)^2 + \left(\frac{\sigma_F}{\tau_F^2}\right)^2} \quad (4)$$

Results

Preparation and characterization of Y_{356}W-photoβ_2

Photoβ_2s are prepared by replacing two surface cysteine residues (C_{268} and C_{305}) with serines, and by replacing a single surface serine (S_{355}) with cysteine. This allows site-specific conjugation of a [Re^I] photooxidant at position 355 by performing an S_N2 reaction with [$Re^I(CO)_3$(phen)($PyCH_2Br$)]PF_6. Here, we have also replaced the adjacent redox-active Y_{356} residue with W. Neither the unlabelled (S_{355}C-Y_{356}W-β_2) nor the labelled ([Re]$_{355}$-Y_{356}W-photoβ_2) constructs exhibit enzymatic activity under steady-state turnover conditions performed in the dark (RNR assay conditions are described in the SI). Measurement of the K_d for the Y_{356}W-photoβ_2:α_2 interaction was performed by a competitive inhibition assay shown in Figure 1. The value of K_d = 0.8 ± 0.1 μM obtained is only slightly larger than that of the wt-α_2:β_2 (0.2 μM)[18] and essentially equal to the K_d = 0.7 ± 0.1 μM measured for the Y-photoβ_2:α_2 interaction.[10]

Photochemistry

Photooxidation of W_{356} can be achieved by two methods schematically represented in Figure 2. Direct excitation (λ_{exc} = 355 nm) of [Re^I] gives rise to a ^{3}[Re^I]* excited state (after intersystem crossing from the initially formed singlet state), which is sufficiently oxidizing and long-lived to directly oxidize an adjacent amino acid, namely W_{356}, to produce a charge-separated state [Re^0]-W•. The kinetics of this process report on the rate of formation of W• and can be assessed by monitoring the emission lifetime of ^{3}[Re^I]*. An additional method for photooxidizing W_{356} is by generating ^{3}[Re^I]* in the presence of a large excess of

$Ru(NH_3)Cl_3$, which functions as a "flash-quencher". In this case, $Ru(NH_3)Cl_3$ oxidatively quenches $^3[Re^I]^*$ to $[Re^{II}]$; the resultant $[Re^{II}]$ is a potent oxidant ($E^{o\prime}$ = 2.07 V, *vide infra*, Figure 2c)[19] capable of oxidizing W_{356} to yield a •W–$[Re^I]$ state. The kinetics of W• (and/or $WH^{\bullet+}$) formation and decay are monitored by transient absorption spectroscopy. The two methods differ primarily in their ability to undergo the reverse reaction, charge-recombination. In the former case, charge recombination within the photochemically generated •W–$[Re^0]$ generates the initial W–$[Re^I]$ state. The rate constant with which •W–$[Re^0]$ is produced by charge-separation, is similar to that with which it returns to W–$[Re^I]$ by charge recombination, thus lowering the yield of the photogenerated radical for spectroscopic analysis. This experimental hurdle is circumvented by using the $Ru(NH_3)Cl_3$ as there is no charge-recombination pathway available with the elimination of $[Re^0]$ upon its reaction with the external Ru^{III} flash quencher. The net result is that the photochemical yield of W• (and/or $WH^{\bullet+}$) is increased, this allowing for the direct observation of spectroscopic signals associated with the radical species.

W and Y amino acids are among the most ubiquitous in facilitating biological ET reactions.[20] In comparing the two, Y is much more likely to undergo a concerted PCET (CPET) reaction[21] due to the extremely acidic nature of the $YH^{\bullet+}$ moiety ($pK_a \approx -2$ [22]). On the contrary, $WH^{\bullet+}$ has a much higher pK_a ($\approx +4.5$)[23] making a stepwise ETPT process also possible at physiological pH. Figure 3 shows the TA spectrum of Y_{356}W-photoβ_2:α_2 (blue circles) collected 8 μs after excitation under flash quench conditions. The TA spectrum of the control Y_{356}F-photoβ_2:α_2 (black circles) was also examined. Here the control Y_{356}F-photoβ_2 serves as a measure of the non-specific photochemical W oxidation, as there are additional W residues within β_2. The λ_{max} observed at 520 nm for the Y_{356}W-photoβ_2:α_2 complex (and for Y_{356}W-photoβ_2, Figure S1) are consistent with the deprotonated W• radical rather than a protonated radical cation ($WH^{\bullet+}$), which typically display an absorption maximum at ~560-580 nm.[24] We do not observe the formation of any significant amount of a $WH^{\bullet+}$ intermediate over the time course (3–20 μs) of radical decay. The sharp absorption feature at 410 nm in Figure 3 is consistent with that of Y•.[12,25,26] Given typical extinction coefficients observed for W• (~2,000 M^{-1} cm^{-1})[24] and Y• (~3,000 M^{-1} cm^{-1})[25] within various enzymes,[1] the ΔOD of 3.3×10^{-3} that we observe in the flash-quenched Y_{356}W-photo$\beta_2\alpha_2$ complex represents a 3- and 7-fold enhancement in the yield of photogenerated radical relative to the 2,3,5-F_3Y- and Y-photoβ_2s respectively.[10,12] When W is replaced by a redox inert F, signatures consistent with W• were also observed but with significantly different spectral character. The flash-quenched Y_{356}F-photo$\beta_2\alpha_2$ construct exhibits a spectrum with a broad signal at λ_{max} ~ 530 nm and a small shoulder at 590 nm (Figure 3, black circles). Additional controls in which the TA spectra of Y_{356}W-photoβ_2 and Y_{356}F-photoβ_2 were measured in the absence of α_2 are shown in Figure S1. In the absence of α_2, the λ_{max} associated with W• was red-shifted to 570 nm, consistent with $WH^{\bullet+}$. These results suggest multiple distinct W oxidation processes which may evolve differently, and appear distinct from the spectrum of the Y_{356}W-photoβ_2:α_2. Another small peak at 410 nm was also observed in the transient spectra of the Y_{356}F-photoβ_2 consistent with a small amount of tyrosine oxidation within β_2 (Figure S1).

Photochemical turnover

In the presence of wt-α_2, substrate (CDP) and effector (ATP), illumination of Y_{356}W-photoβ_2 results in dCDP formation. Here, the total number of dCDP produced is limited by the amount of α_2 present. Re-reduction of the four participating cysteine residues in α_2 is required for additional turnovers. Typically these reducing equivalents are supplied by coupled reactions with thioredoxin, thioredoxin reductase, and NADPH. In the absence of such a reducing system a "single turnover" gives a theoretical maximum of 4 dCDP/α_2. Figure 4 shows the results of photochemically driven single turnovers, both in the presence and absence of flash quencher. Greater turnover numbers (20% relative to wt-β_2 under the same conditions) are observed with the $Ru(NH_3)_6^{3+}$ flash-quench reagent (burgundy bar), presumably owing to the longer lifetime of the oxidatively quenched state as compared to using the excited state (purple bar) as the oxidant (4% turnover relative to wt-β_2 under the same conditions). We note that the wt experiments were performed with a β_2 that retains the native Y• cofactor (has not been reduced with HU) and lacks a [Re^I] photosensitizer, thus representing a single turnover experiment performed under the conditions of the photochemical experiments. No turnover is observed for the Y_{356}W-photoβ_2:α_2 complex in the dark (blue bar) or if a radical block is placed in the PCET pathway (Y → F at position 356 in β or 731 in α). This observation is consistent with the distinction between the spectral signatures of Y_{356}W- and Y_{356}F-photoβ_2 constructs (Figure 3). Of the five photoβ_2 constructs previously reported (Y-, 3,5-F_2Y-, 2,3-F_2Y-, 2,3,5-F_3Y- and 2,3,6-F_3Y-photoβ_2), the Y_{356}W-photoβ_2 variant displays photochemical turnover activity second only to that in which the native Y residue is retained at position 356.[13] As noted previously, the K_{Ds} for Y- and Y_{356}W-photoβ_2 constructs are similar. Thus, the slightly decreased activity of Y_{356}W-photoβ_2 relative to Y-photoβ_2 is not a function of weaker binding affinity for the α_2 subunit.

PCET Kinetics

The single wavelength kinetics decay curve of the photogenerated W• as probed by TA spectroscopy is shown in Figure 5. Formation of W• monitored at 520 nm could not be observed directly by TA spectroscopy due to spectral and temporal overlap with the ^{3}[Re^I]* emission (λ_{max} ~ 540 nm), even under flash-quench conditions. To address this, we examined the quenching kinetics of the ^{3}[Re^I]* excited state in the presence of W by time-resolved emission spectroscopy (Table 1). To calculate the quenching rate constant, we measured the ^{3}[Re^I]* excited state lifetime in Y_{356}W-photoβ_2 (τ_W) and Y_{356}F-photoβ_2 (τ_F). Substituting these lifetime values into Eq. 3 furnishes the rate constant of $k_q = 4.4 \pm 0.2 \times 10^5\ s^{-1}$ for the quenching of ^{3}[Re^I]* by W oxidation in the presence of wt-α_2.

The W• radical observed in the TA spectrum of Y_{356}W-photoβ_2:α_2 decays with a rate constant of $4.4 \pm 0.2 \times 10^4\ s^{-1}$ (Figure 5). This rate constant is in-line with our previous observations using other photoβ_2s in the presence of wt-α_2.[12] Unlike Y- and F_3Y-photoβ_2s, neither the absence of wt-α_2, nor the presence of Y_{731}F-, 3,5-F_2Y_{731}- or 2,3,5-F_3Y_{731}-α_2 result in significant changes in these kinetics. In the case of the Y_{356}W-photoβ_2, disruption of the PCET pathway is apparent from comparing the data in the top and bottom halves of Table 1; there is no enhancement in k_q measured in the presence of wt- versus Y_{731}F-α_2. In contrast, with Y-photoβ_2 a ~24% enhancement in k_q for the intact PCET pathway is observed relative to the case with the pathway blocked at position α_{731}.[10] These data suggest

that the difference in reactivity between W_{356}-photoβ_2 and Y_{356}-photoβ_2 result from a misalignment or disruption of the PCET pathway incurred upon replacing Y_{356} with W.

Discussion

The Y_{356}W-β_2 construct of *E. coli* RNR has previously been shown to have no enzymatic activity, even when assayed *in vivo* by highly sensitive screening method.[27] We also observe that Y_{356}W-β_2, and the unlabeled-Y_{356}W-photoβ_2 containing the three mutations necessary for the production of photoβ_2s (C_{268}S, C_{305}S and S_{355}C), are inactive. The only activity observed arises from low amounts of endogenous wt-β_2 present as a result of the fact that RNR is an essential enzyme. The inactivity of these Y $\rightarrow$ W-β_2 variants may result simply from perturbation of the β_{356} reduction potential, since progressively lower activity is measured for RNRs with F_nYs incorporated at position β-356 as the $E^{\circ\prime}$(F_nY•/ F_nY–) approach that of $E^{\circ\prime}$(WH•$^+$/WH).[28] Another explanation for the observed inactivity may be due to a misalignment of the PCET pathway. We have shown that this inactivity may be overcome by photogeneration of W•. As shown in Figure 4, Y_{356}W-photoβ_2 is active for turnover under illumination. The photochemical system possesses significant overpotential for W• generation and hence the barriers to the generation of a •W_{356} are overcome and forward radical propagation into α_2 becomes possible in the photo RNR.

The two methods employed to photogenerate the W• radical are schematically described in Figure 2. The W• radical may be photogenerated by direct oxidation from the triplet excited state of the [Re] complex (^{3}[Re^I]*) (Figure 2a) or by oxidation from the [Re^{II}] complex, produced by the flash-quench method (Figure 2b). The energetics associated with the [Re] complex of the two different pathways is summarized in Figure 2c. The rate constant for W oxidation, as measured by emission quenching, of 4.4 ± 0.2 × 10^5 s^{-1}, is very similar to that of Y• or F_nY• formation,[10,12] despite their significant differences in ΔG°.

The rate constant for W oxidation is consistent with an ET process, as opposed to a PCET process, and accordingly follows a Marcus formalism described in equation Eq. 5,

$$k_{ET} = \frac{2\pi H_{DA}^2}{\hbar\sqrt{4\pi\lambda k_B T}} \cdot e^{-\frac{(\lambda+\Delta G^{\circ})^2}{4\lambda k_B T}} \quad (5)$$

Figure 6 plots the previously measured rate constants for radical formation in a series of F_nY-photoβ_2s (n = 0–3) within the photoRNR complex. Over the pH regime examined, the F_nYs are deprotonated and radical generation in β-F_nY_{356} occurs by ET. Moreover, the PCET process for Y oxidation in the presence of α_2 also behaves kinetically like an ET process owing to fast proton transfer from the interface. As is clearly evident from the Marcus plot, the ET process for radical generation within the F_nY-photoβ_2:α_2 complex occurs in the Marcus inverted regime, where an increase in $|-\Delta G^{\circ\prime}|$ results in a decrease in k_q.[13] The F_nY-photoβ_2 series has now been expanded to include k_q measured for the Y_{356}W-photoβ_2:α_2 complex, assuming similar H_{DA} and λ parameters between the mutations. Based on the E° of 1.15 V (vs NHE) for WH•$^+$ + e^- $\rightarrow$ WH measured by differential pulse voltammetry,[29] and an excited state reduction potential for [Re^I]* $\rightarrow$ [Re^0] of 1.94 V vs

NHE (Figure 2c),[13] we calculate the $-\Delta G^{\circ\prime}$ for W oxidation of 0.79 V. At this potential, the measured rate constant from the [Re^{I}]* quenching experiment of $4.4 \pm 0.2 \times 10^{5}$ s^{-1} falls on the Marcus curve in Figure 6. This result indicates that tryptophan oxidation proceeds by ET to furnish $WH^{\bullet+}$. We note, however, that the TA spectrum of Figure 3 is that of W• as opposed to $WH^{\bullet+}$. Together, the quenching and TA kinetics indicate an ET/PT process in which rate-limiting ET precedes rapid proton loss to produce W•. The fast proton loss is consistent with the ΔpK_a of 3.1 between $WH^{\bullet+}$ and bulk solution (pH = 7.6).

Finally, a reorganization energy of $\lambda = 1$ eV is determined for the ET process at the photoRNR α_2/β_2 interface. This value is 0.9 eV lower than that determined for [Re^{I}]-F_nY model complexes in solution,[30] revealing that the enzyme microenvironment exerts a significant influence in minimizing the reorganization energy. Similar reductions in the reorganization energy have been observed for Cu enzymes as compared to Cu metal complexes,[31] and more generally for a host of metallocofactors embedded within protein matrices. [32]

Conclusions

W and Y are among the most common amino acids to facilitate biological ET reactions.[1,22] In comparing the two, Y is much more likely to undergo a concerted PCET (CPET) reaction due to the extremely acidic nature of the $YH^{\bullet+}$ moiety ($pK_a \approx -2$). The much higher pK_a of $WH^{\bullet+}$ ($\approx +4.5$) makes a stepwise ET/PT process possible at physiological pH as we observe here. A concerted PCET mechanism has been proposed in rare instances for model complexes,[33] but to our knowledge this has not been observed in a biological system. The formation of W• at β_{356} obeys a Marcus formalism indicating that W_{356}-photoβ_2 oxidation proceeds through $WH^{\bullet+}$. The appearance of W• in the TA spectrum points to fast proton loss, indicating an ET/PT mechanism for radical generation in the Y_{356}W-photoβ_2:α_2 complex. Conversely, radical generation in Y_{356}-photoβ_2 proceeds by a concerted PCET process, facilitated by protein-mediated PT.[13] Radical generation in Y_{356}- and W-photoβ_2 are also distinguished by their dependence of the PCET pathway. Photogeneration of W• is insensitive to radical blocks within the PCET pathway whereas Y• photogeneration is attenuated by the presence of the radical block. Together, these results indicate that the PCET events required for the formation of an amino acid radical at β_{356} are precisely controlled within the RNR protein-protein interface.

Supplementary Material

Refer to Web version on PubMed Central for supplementary material.

Acknowledgements

LO acknowledges the National Science Foundation's Graduate Research Fellowship Program. This research was supported by the U.S. National Institute of Health Grant GM047274 (DGN) and GM029595 (JS).

Abbreviations

RNR *E. coli* class Ia ribonucleotide reductase

α_2	large subunit of RNR containing substrate and effector binding sites
β_2	small subunit of RNR containing the diiron-tyrosyl radical cofactor
PCET	proton-coupled electron transfer
[Re^I]	methylpyridyl rhenium(I) tricarbonyl phenanthroline phosphorushexafluorate complex
photoβ_2	$C_{268}S/C_{305}S/S_{355}C$-$\beta_2$ appended with [Re^I]
W-photoβ_2	$C_{268}S/C_{305}S/S_{355}C/Y_{356}W$-$\beta_2$ appended with the [Re^I] complex
TA	transient absorption
MALDI-TOF	matrix-assisted laser desorption/ionization-time of flight
MLCT	metal-to-ligand charge transfer
HU	hydroxyurea
ATP	adenosine 5′-triphosphate
CDP	cytidine 5′-diphosphate
[^{3}H]-CDP	5-tritiated cytidine 5′-diphosphate sodium salt hydrate
HEPES	4-(2-hydroxyethyl)-piperazin-1-ylethanesulphonic acid
TR	thioredoxin
TRR	thioredoxin reductase
AP	calf alkaline phosphatase

References

(1). Stubbe J, van der Donk WA. Protein Radicals in Enzyme Catalysis. Chem. Rev. 1998; 98:705–762. [PubMed: 11848913]

(2). Brown NC, Reichard P. Role of Effector Binding of Allosteric Control of Ribonucleoside Diphosphate Reductase. J. Mol. Biol. 1969; 46:25–38. [PubMed: 4902211]

(3). Uhlin U, Eklund H. Structure of Ribonucleotide Reductase Protein R1. Nature. 1994; 370:533–539. [PubMed: 8052308]

(4). Bennati M, Robblee JH, Mugnaini V, Stubbe J, Freed JH, Borbat P. EPR Distance Measurements Support a Model for Long-Range Radical Initiation in *E. coli* Ribonucleotide Reductase. J. Am. Chem. Soc. 2005; 127:15014–15015. [PubMed: 16248626]

(5). Stubbe J, Nocera DG, Yee CS, Chang MCY. Radical Initiation in the Class I Ribonucleotide Reductase: Long-Range Proton-Coupled Electron Transfer? Chem. Rev. 2003; 103:2167–2202. [PubMed: 12797828]

(6). Minnihan EC, Nocera DG, Stubbe J. Reversible, Long-Range Radical Transfer in *E. coli* Class Ia Ribonucleotide Reductase. Acc. Chem. Res. 2013; 46:2524–2535. [PubMed: 23730940]

(7). Ge J, Yu G, Ator MA, Stubbe J. Pre-Steady-State and Steady-State Kinetic Analysis of *E. coli* Class I Ribonucleotide Reductase. Biochemistry. 2003; 42:10071–10083. [PubMed: 12939135]

(8). Chang MCY, Yee CS, Stubbe J, Nocera DG. Turning On Ribonucleotide Reductase by Light-Initiated Amin o Acid Radical Generation. Proc. Natl. Acad. Sci. U.S.A. 2004; 101:6882–6887. [PubMed: 15123822]

(9). Holder PG, Pizano AA, Anderson BL, Stubbe J, Nocera DG. Deciphering Radical Transport in the Large Subunit of Class I Ribonucleotide Reductase. J. Am. Chem. Soc. 2012; 134:1172–1180. [PubMed: 22121977]

(10). Pizano AA, Olshansky L, Holder PG, Stubbe J, Nocera DG. Modulation of Y356 Photooxidation in *E. coli* Class Ia Ribonucleotide Reductase by Y731 Across the α2:β2 Interface. J. Am. Chem. Soc. 2013; 135:13250–13253. [PubMed: 23927429]

(11). Pizano AA, Lutterman DA, Holder PG, Teets TS, Stubbe J, Nocera DG. Photo-Ribonucleotide Reductase β2 by Selective Cysteine Labelling with a Radical Phototrigger. Proc. Natl. Acad. Sci. U.S.A. 2012; 109:39–43. [PubMed: 22171005]

(12). Olshansky L, Pizano AA, Wei Y, Stubbe J, Nocera DG. Kinetics of Hydrogen Atom Abstraction from Substrate by an Active Site Thiyl Radical in Ribonucleotide Reductase. J. Am. Chem. Soc. 2014; 136:16210–16216. [PubMed: 25353063]

(13). Olshansky L, Stubbe J, Nocera DG. Charge-Transfer Dynamics at the α/β Subunit Interface of a Photochemical Ribonucleotide Reductase. J. Am. Chem. Soc. 2015; 138:1196–1205. [PubMed: 26710997]

(14). Minnihan EC, Seyedsayamdost MR, Uhlin U, Stubbe J. Kinetics of Radical Intermediate Formation and Deoxynucleotide Production in 3-Aminotyrosine-Substituted *Escherichia coli* Ribonucleotide Reductases. J. Am. Chem. Soc. 2011; 133:9430–9440. [PubMed: 21612216]

(15). Chivers PT, Prehoda KE, Volkman BF, Kim BM, Markley JL, Raines RT. Microscopic p*K*a Values of *Escherichia coli* Thioredoxin. Biochemistry. 1997; 36:14985–14991. [PubMed: 9398223]

(16). Lunn CA, Kathju S, Wallace BJ, Kushner SR, Pigiet V. Amplification and Purification of Plasmid-encoded Thioredoxin from *Escherichia coli* K12. J. Biol. Chem. 1984; 259:10469–10474. [PubMed: 6381486]

(17). Steeper JR, Steuart CD. A Rapid Assay for CDP Reductase Activity in Mammalian Cell Extracts. Anal. Biochem. 1970; 34:123–130. [PubMed: 5440901]

(18). Climent I, Sjöberg B-M, Huang CY. Electron Transfer Associated with Oxygen Activation in the β2 Protein of Ribonucleotide Reductase from *Escherichia coli*. Biochemistry. 1991; 30:5164–5171. [PubMed: 2036382]

(19). Dattelbaum DM, Omberg KM, Schoonover JR, Martin RL, Meyer TJ. Application of Time-Resolved Infrared Spectroscopy to Electronic Structure in Metal-to-Ligand Charge-Transfer Excited States. Inorg. Chem. 2002; 41:6071–6079. [PubMed: 12425635]

(20). Migliore A, Polizzi NF, Therien MJ, Beratan DN. Biochemistry and Theory of Proton-Coupled Electron Transfer. Chem. Rev. 2014; 114:3381–3465. [PubMed: 24684625]

(21). Mayer JM. Proton Coupled Electron Transfer: A Reaction Chemist's View. Annu. Rev. Phys. Chem. 2004; 55:363–390. [PubMed: 15117257]

(22). Harriman A. Further Comments on the Redox Potentials of Tryptophan and Tyrosine. J. Phys. Chem. 1987; 91:6104–6106.

(23). Posener ML, Adams GE, Wardman P, Cundall RB. Mechanism of Tryptophan Oxidation by some Inorganic Radical-Anions: A Pulse Radiolysis Study. J. Chem. Soc. Faraday Trans. 1976; 1:2231–2239. 32.

(24). Solar S, Getoff N, Surdhar PS, Armstrong DA, Singh A. Oxidation of Tryptophan and N-Methylindole by $N_3^{\bullet}$, $Br_2^{\bullet-}$, and $(SCN)_2^{\bullet-}$ Radicals in Light- and Heavy-Water Solutions: A Pulse Radiolysis Study. J. Phys. Chem. 95:3639–3643.

(25). Bansal K, Fessenden RW. Pulse Radiolysis Studies of the Oxidation of Phenols by $SO_4^{\bullet-}$ and $Br_2^{\bullet-}$ in Aqueous Solutions. Radiat. Res. 1976; 67:1–8. [PubMed: 940923]

(26). Seyedsayamdost MR, Reece SY, Nocera DG, Stubbe J. Mono-, Di-, Tri-, and Tetra-Substituted Fluorotyrosines: New Probes for Enzymes that Use Tyrosyl Radicals in Catalysis. J. Am. Chem. Soc. 2006; 128:1569–1579. [PubMed: 16448128]

(27). Ekberg M, Birgander P, Sjöberg B-M. *In Vivo* Assay for Low-Activity Mutant Forms of *Escherichia coli* Ribonucleotide Reductase. J. Bacteriol. 2003; 185:1167–1173. [PubMed: 12562785]

(28). Seyedsayamdost MR, Yee CS, Reece SY, Nocera DG, Stubbe J. pH Rate Profiles of FnY356–R2s (n = 2, 3, 4) in *Escherichia coli* Ribonucleotide Reductase: Evidence that Y356 Is a Redox-Active Amino Acid along the Radical Propagation Pathway. J. Am. Chem. Soc. 2006; 128:1562–1568. [PubMed: 16448127]

(29). Zhang M-T, Hammarström L. Proton-Coupled Electron Transfer from Tryptophan: A Concerted Mechanism with Water as Proton Acceptor. J. Am. Chem. Soc. 2011; 133:8806–8809. [PubMed: 21500853]

(30). Reece SY, Seyedsayamdost MR, Stubbe J, Nocera DG. Electron Transfer Reactions of Fluorotyrosyl Radicals. J. Am. Chem. Soc. 2006; 128:13654–13655. [PubMed: 17044670]

(31). Gray HB, Malmstrom BG, Williams RJP. Copper Coordination in Blue Proteins. J. Biol. Inorg. Chem. 2000; 5:551–559. [PubMed: 11085645]

(32). Liu J, Chakraborty S, Hosseinzadeh P, Yu Y, Tian S, Petrik I, Bhagi A, Lu Y. Metalloproteins Containing Cytochrome, Iron-Sulfur, or Copper Redox Centers. Chem. Rev. 2014; 114:4366–4469. [PubMed: 24758379]

(33). Dongare P, Maji S, Hammarström L. Direct Evidence of a Tryptophan Analogue Radical Formed in a Concerted Electron–Proton Transfer Reaction in Water. J. Am. Chem. Soc. 2016; 138:2194–2199. [PubMed: 26871741]

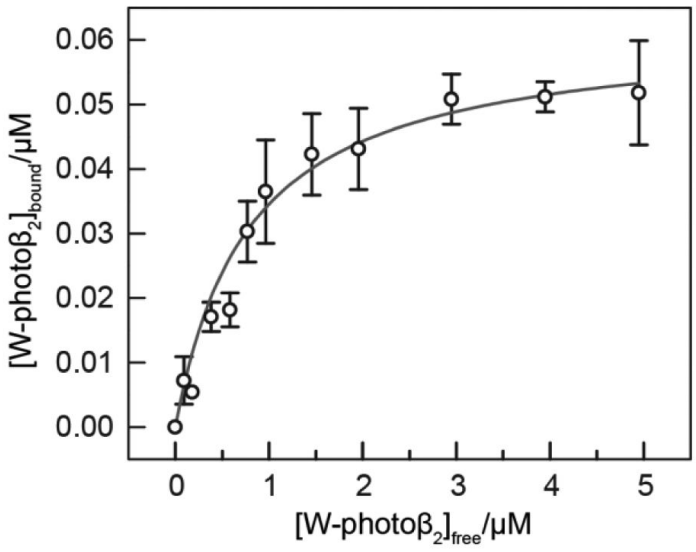

Figure 1.

Subunit affinity (K_D) of the Y_{356}W-photoβ_2:α_2 complex was assessed by adding increasing amounts of Y_{356}W-photoβ_2 to reaction mixtures of wt–$\alpha_2\beta_2$, and measuring the specific activities (SAs) for each reaction. In a final volume of 300 μL, each reaction contained 0.2 μM wt-β_2, 0.1 μM wt-α_2, Y_{356}W-photoβ_2 (0–5 μM), 30 μM TR, 0.5 μM TRR, 1 mM CDP, 3 mM ATP, 0.2 mM NADPH in assay buffer, where the absorbance decrease at 340 nm representing consumption of NADPH was used to determine SA. Data were analyzed as previously reported, to give a K_D of 0.8 ± 0.1 μM where the error bars represent 1 s.d. from duplicate measurements.

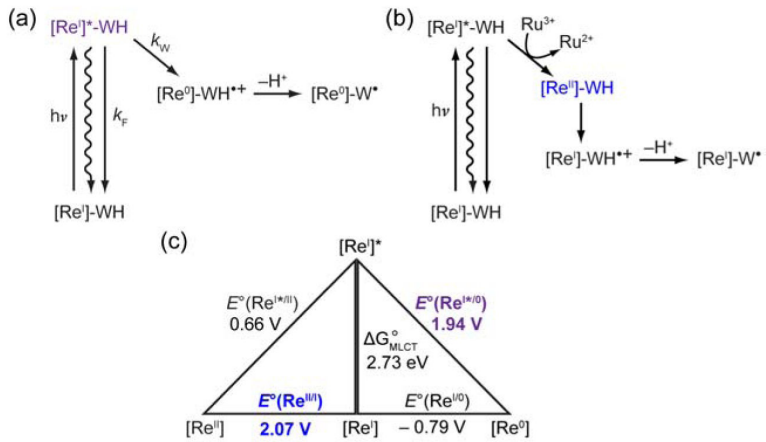

Figure 2.

Photophysical schemes describing the photogeneration of W• by (a) direct quenching of the excited state of the [Re] complex ([Re^{I}*]) and (b) by the oxidized [Re^{II}] complex furnished from the flash-quench method. (c) Latimer diagram describing of the energetics relevant to the direct quenching and flash-quench pathways.

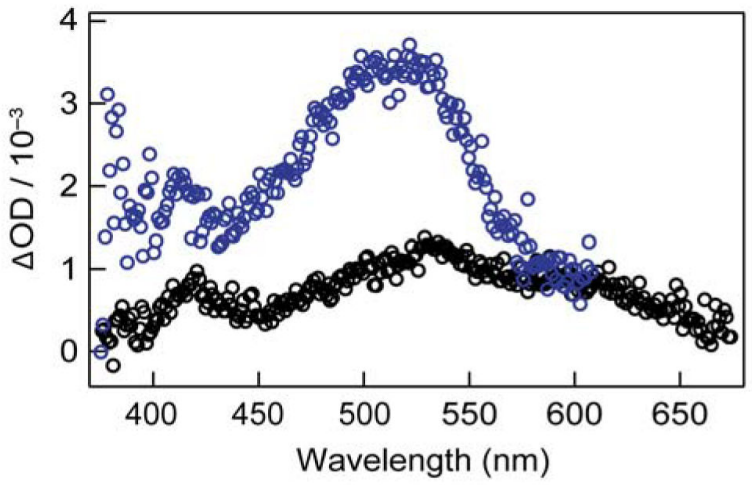

Figure 3.

TA spectra of Y_{356}W- and Y_{356}F-photoβ_2 alone and in complex with α_2 collected 8 μs after the 355 nm excitation pulse. The displayed spectra are averages of 3 independently prepared samples, containing either 75 μM wt-α_2 and 50 μM Y_{356}W-photoβ_2 or 50 μM wt-α_2 and 30 μM Y_{356}F-photoβ_2 (blue and black, respectively). Samples also contained 1 mM CDP, 3 mM ATP, and 10 mM $Ru(NH_3)_6Cl_3$, in assay buffer at pH 7.6.

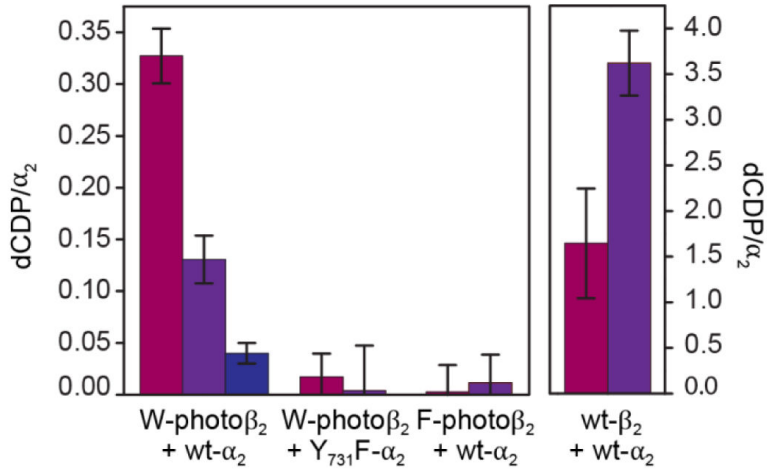

Figure 4.

Photochemical single turnover experiments in the presence (burgundy) and absence (purple) of 10 mM $Ru(NH_3)_6Cl_3$ relative to experiments performed in the dark (blue). Samples contained 10 μM or 20 μM of Y_{356}W-photoβ_2, Y_{356}F-photoβ_2 or wt-β_2 (containing the native tyrosyl radical at 1.2 Y•/β_2 and lacking the [Re^I] photosensitizer), and 10 μM Y_{731}F- or wt-α_2 as indicated, 0.2 mM [5-^{3}H]-CDP (26,700 cpm/nmol), and 3 mM ATP, in assay buffer at pH 7.6. Error bars represent 1 s.d. from triplicate measurements on independently prepared samples.

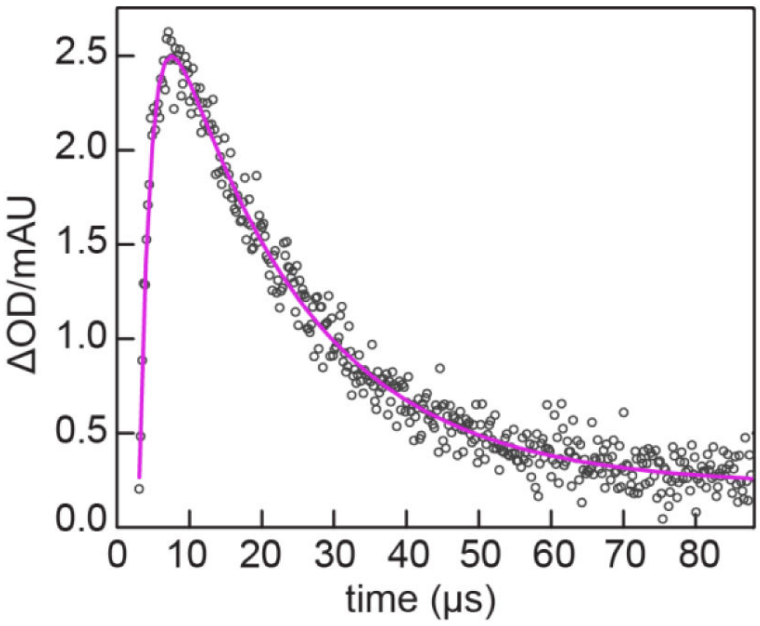

Figure 5.

Single wavelength TA kinetics centered at 520 ± 1 nm for an average of 3 samples, each containing 50 μM Y_{356}W-photoβ_2, 75 μM wt-α_2, 1 mM CDP, 3 mM ATP, 10 mM $Ru(NH_3)_6Cl_3$, in assay buffer at pH 7.6. The pink line is a fit of the data to Eq. 1, yielding rate constants of 6.6 ± 0.4 × 10^5 s^{-1} for the growth, and 4.4 ± 0.2 × 10^4 s^{-1} for decay of the W• signal. The growth signal is convoluted with the photoβ_2 emission, and thus may not represent the actual rate of formation of W_{356}•.

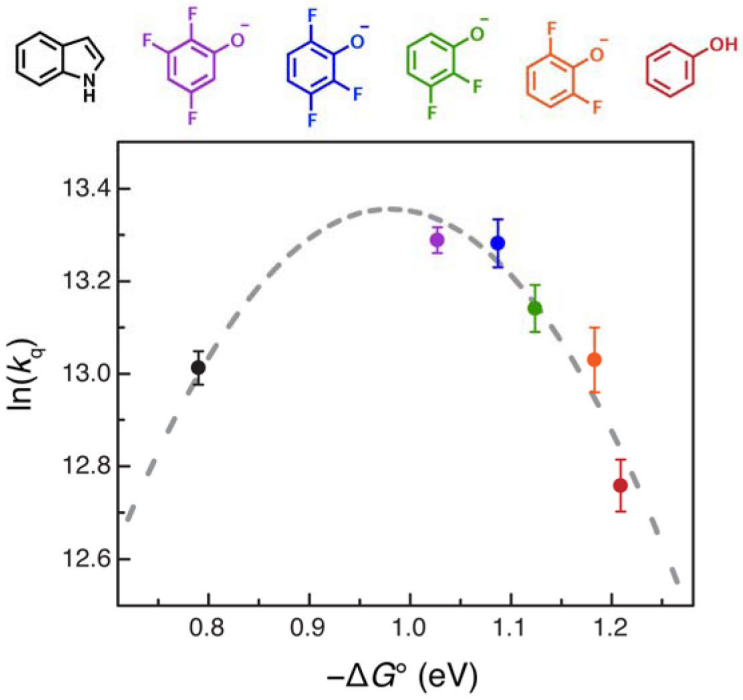

Figure 6.

Correlation of the natural log of k_q with $-\Delta G°$ for charge-separation within the photoβ_2:α_2 complexes with the specified residue at position 356. Dashed lines represent simulations to the semi-classical Marcus equation (described in ref 13) with r = 12.5 Å, λ = 0.98 eV, and H_{DA} = 0.051 cm–1. All data except that of Y_{356}W-photoβ_2 (black, Table 1, calculated according to Eq. 3) are reproduced from ref 13. Error bars represent 1 s.d. for triplicate measurements on independently prepared samples, calculated according to Eq. 4.

Table 1

Pathway-Dependent Excited-State Quenching at the Y_{356}W-photoβ_2:α_2 Subunit Interface

Interface Residues		^{3}[Re^I]* Lifetime[a]	Quenching Rate Constant
β_{356}	α_{731}	τ / ns	k_q / 10^5 s^{-1}
W	Y	549 (4)	4.4 (2)
F	Y	725 (8)	
W	F	565 (2)	4.1 (2)
F	F	733 (11)	

[a] Emission lifetimes measured on samples of 10 μM Y_{356}W-photoβ_2 or Y_{356}F-photoβ_2 and 25 μM wt-α_2 or Y_{731}F-α_2 (as indicated), 1 mM CDP and 3 mM ATP in assay buffer at pH 7.6, λ_{exc} = 355 nm, λ_{det} = 600 nm. k_q calculated according to Eq. 3. Representative decay traces shown in Figure S2. Error limits shown in parentheses represent 1 s.d. from triplicate measurements on independently prepared samples.